analytical chemistry

pubs.acs.org/ac Article

Pomegranate-Inspired Silica Nanotags Enable Sensitive Dual-Modal Detection of Rabies Virus Nucleoprotein

Jiaojiao Zhou,[§] Meishen Ren,[§] Wenjing Wang, Liang Huang, Zhicheng Lu, Zhiyong Song, Mohamed F. Foda, Ling Zhao,* and Heyou Han*

Cite This: https://dx.doi.org/10.1021/acs.analchem.0c00200 Read Online

ACCESS | Metrics & More | Article Recommendations | * Supporting Information

ABSTRACT: The outbreak of rabies virus (RABV) in Asia and Africa has attracted widespread concern due to its 100% mortality rate, and RABV detection is crucial to its diagnosis and treatment. Herein, we report a sensitive and reliable strategy for the dual-modal RABV detection using pomegranate-shaped dendritic silica nanospheres fabricated with densely incorporated quantum dots (QDs) and horseradish peroxidase (HRP)-labeled antibody. The immunoassay involves the specific interaction between virus and nanospheres-conjugated antibody coupled with robust fluorescence signal originating from QDs and naked-eye discernible colorimetric signal on the oxTMB. The ultrahigh loading capacity of QDs enables the detection limit down to 8 pg/mL via fluorescence modality, a 348-fold improvement as compared with conventional enzyme-linked immunosorbent assay (ELISA). In addition, the detection range was from 1.20×10^2 to 2.34×10^4 pg/mL by plotting the absorbance at 652 nm with RABV concentrations with a detection limit of 91 pg/mL, which is nearly 2 order of magnitude lower than that of the conventional ELISA. Validated with 12 brain tissue samples, our immunoassay results are completely consistent with polymerase chain reaction (PCR) results. Compared with the PCR assay, our approach requires no complex sample pretreatments or expensive instruments. This is the first report on RABV diagnosis using nanomaterials for colorimetry-based prescreening and fluorescence-based quantitative detection, which may pave the way for virus-related disease diagnosis and clinical analysis.

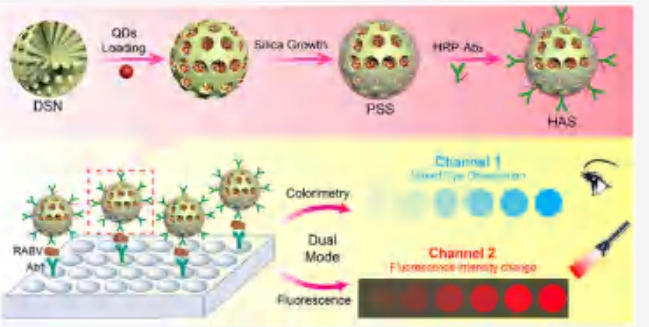

Rabies virus (RABV), one kind of neurotropic viruses with a 100% mortality rate in humans and animals,[1] can infect the central nervous system of all warm-blooded animals,[2] cause acute encephalomyelitis and ultimately death,[3] and thus severely threaten human health and life with devastating effects.[4,5] According to the data from the World Health Organization (WHO) in 2018, rabies causes nearly 59 000 human deaths annually worldwide, with Asia accounting for 59.6% of the total.[6] In addition, rabies can usually be validated in the late stage of disease or postmortem due to the dependence of its prognosis on exposure history and clinical findings.[7] Therefore, to prevent the virus spread and the disease outbreak, it is essential to develop timely and reliable methods for early virus detection and prognosis evaluation.

The difficulties in RABV detection are attributed to its low abundance, main distribution in brain tissues, and transmission to all mammals. Conventional detection methods mainly include the direct fluorescent antibody test (DFAT) and the mouse inoculation test (MIT).[8] Despite their high sensitivity and specificity, DFAT requires well-trained personnel and an expensive fluorescence microscope, and it may also yield false negative results when the brain tissue starts to decompose.[9] Meanwhile, MIT requires animal facilities and is time consuming (up to 28 days).[10] The disadvantages of the traditional detection methods have promoted the development of genomic methods for rabies diagnosis. Quantification of viral RNA can be used as an alternative or to confirm DFA negative results. RABV genome encodes the nucleoprotein (N), and the N gene is the most conserved region in the RABV genome, which has been identified as a diagnostic marker.[7] Viral RNA can be efficiently quantified by PCR-based methods, such as reverse transcription polymerase chain reaction (RT-PCR),[11] real-time RT-PCR,[12] heminested RT-PCR (hnRT-PCR),[13] and so forth. Despite their increasing use, these amplification methods are not recommended by the WHO due to false positive results.[14] Furthermore, these methods require expensive experimental setups, professional staff, and nucleic acid extraction, limiting their applications in the point-of-care area. Thus, it is urgent to develop a simple,

Received: January 15, 2020
Accepted: May 26, 2020
Published: May 26, 2020

Scheme 1. Schematic Illustration of Dual-Modal RABV Immunoassay Based on Pomegranate-Inspired Silica Nanospheres

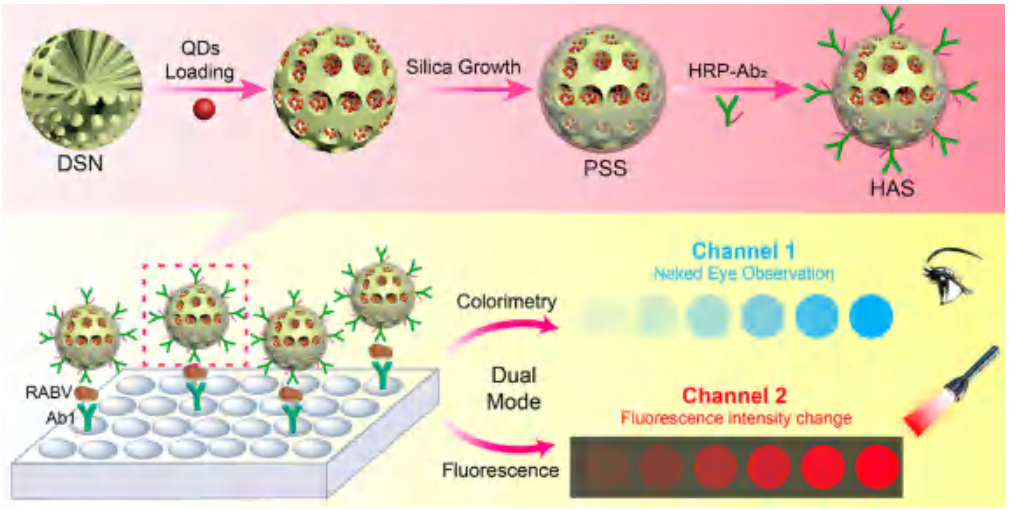

sensitive, and accurate method for virus clinical diagnosis, especially in resource-constrained areas.

Recent advances in nanomaterials and colorimetric analytical strategies offer opportunities for accurate and reliable virus diagnosis without the requirement of sophisticated instruments.[15−20] However, these assays follow a single-modal signal readout, which can be compromised in complex samples and almost fade in precise and highly sensitive diagnosis. With the advancement of inorganic QDs and organic fluorophores, fluorescent materials have been widely employed in biodetection with enhanced sensitivity relative to colorimetric assay.[21−23] Unfortunately, the assays based on organic fluorescent materials suffered from high background fluorescence and an aggregation-caused quenching (ACQ) effect.[24,25] Unlike traditional organic fluorophores, QDs feature the advantages of prominent photostability,[26−29] outstanding brightness,[30,31] and tunable emission spectrum,[32,33] leading to their popular use in biodetection,[34−39] biotracking,[40−42] and biotherapy.[43−45] Inspired by the above results, we speculate novel QDs-based nanomaterials coupled with colorimetry can be used to achieve dual-modal biosensing.

Herein, we report a sensitive RABV immunoassay with fluorescent and colorimetric dual-modal detection based on pomegranate-shaped silica nanospheres (PSS) with densely packed QDs and the conjugated HRP-labeled antibody (HRP-Ab2) (Scheme 1). Specifically, we first synthesized uniform monodispersed dendritic silica nanospheres (DSN) for QDs encapsulation. Compared with traditional QDs coated on the surface silica structure via electrostatic attraction, DSN with highly accessible mesopore channels enabled the encapsulation of large numbers of QDs via the strong thiol−metal coordination, thus enhancing the fluorescence brightness for highly sensitive fluorescence-based biodetection. Then the growth of a dense silica shell on DSN for protection and functionalization is different from those QDs-coated silica nanospheres, which showed reduced fluorescence due to the partial quenching of biomolecules.[46,47] As the nucleoprotein (N) of RABV is the most highly conserved protein,[7] it is significant to detect nucleoprotein for RABV clinical diagnosis. The RABV nucleoprotein-based dual-modal assay was developed by immobilizing HRP-Ab2 on the surface of PSS as a dual-signal probe. The PSS with a large surface-to-volume ratio not only allows the conjugation with a greater amount of HRP-Ab2 but also endows the conjugated HRP-Ab2 with high accessibility to RABV antigens from all sides, enabling the colorimetric signal to be amplified in a constrained area. As illustrated in Scheme 1, the sandwich-structure immunocomplexes were formed between RABV antigen and anti-RABV antibody. After adding TMB and H_2O_2, an obvious color change was observed due to the oxidation of TMB (Channel 1 in Scheme 1). Moreover, thanks to the bright fluorescence of monodisperse PSS, RABV can also be monitored by measuring the fluorescence intensity of the bottom sandwich complex (Channel 2 in Scheme 1). This assay was further validated with brain tissue samples and was identified as an efficient quantitative tool for virus diagnosis with satisfactory sensitivity and accuracy. This is the first report on RABV detection using nanomaterials via the naked eye for preliminary screening and fluorescence for quantitative detection, which will pave the way for virus-related disease diagnosis and clinical analysis.

EXPERIMENTAL SECTION

Materials and Reagents. All reagents and apparatus are provided in the Supporting Information.

Preparation of DSN. Dendritic silica nanospheres were prepared according to the previous report.[48] First, 0.380 g of CTAB, 0.168 g of sodium salicylate, and 0.068 g of TEA were added to 25 mL of water with gentle stirring for 1 h; then 2 mL of TEOS was added to the above solution and kept stirring for 2 h at 80 °C. Then the products were extracted with HCl and methanol solution at 60 °C for 6 h to remove the template, followed by drying in vacuum at room temperature overnight. The collected products were finally dispersed in 100 mL of ethanol. For surface grafting with mercapto groups, the above solution was added with 2.5 mL of ammonia and 1 mL of MPS, followed by continuous stirring for 12 h at room temperature. The final products were collected by centrifugation, washed with ethanol, and dispersed in 50 mL of ethanol.

Preparation of PSS. A 1 mL amount of above ethanol solution was injected to 1 mL of 10 mg/mL QDs with sonication for 5 min. Then the mixture were centrifuged and washed three times to remove excess QDs. This precipitate was dissolved in 200 μL of OTMS under sonication and then added with 15 mL of methanol and 375 μL of ammonia. To grow a silica shell by the Stöber method, the above composites were mixed with 40 mL of ethanol, 1.25 mL of ammonia, and

https://dx.doi.org/10.1021/acs.analchem.0c00200
Anal. Chem. XXXX, XXX, XXX−XXX

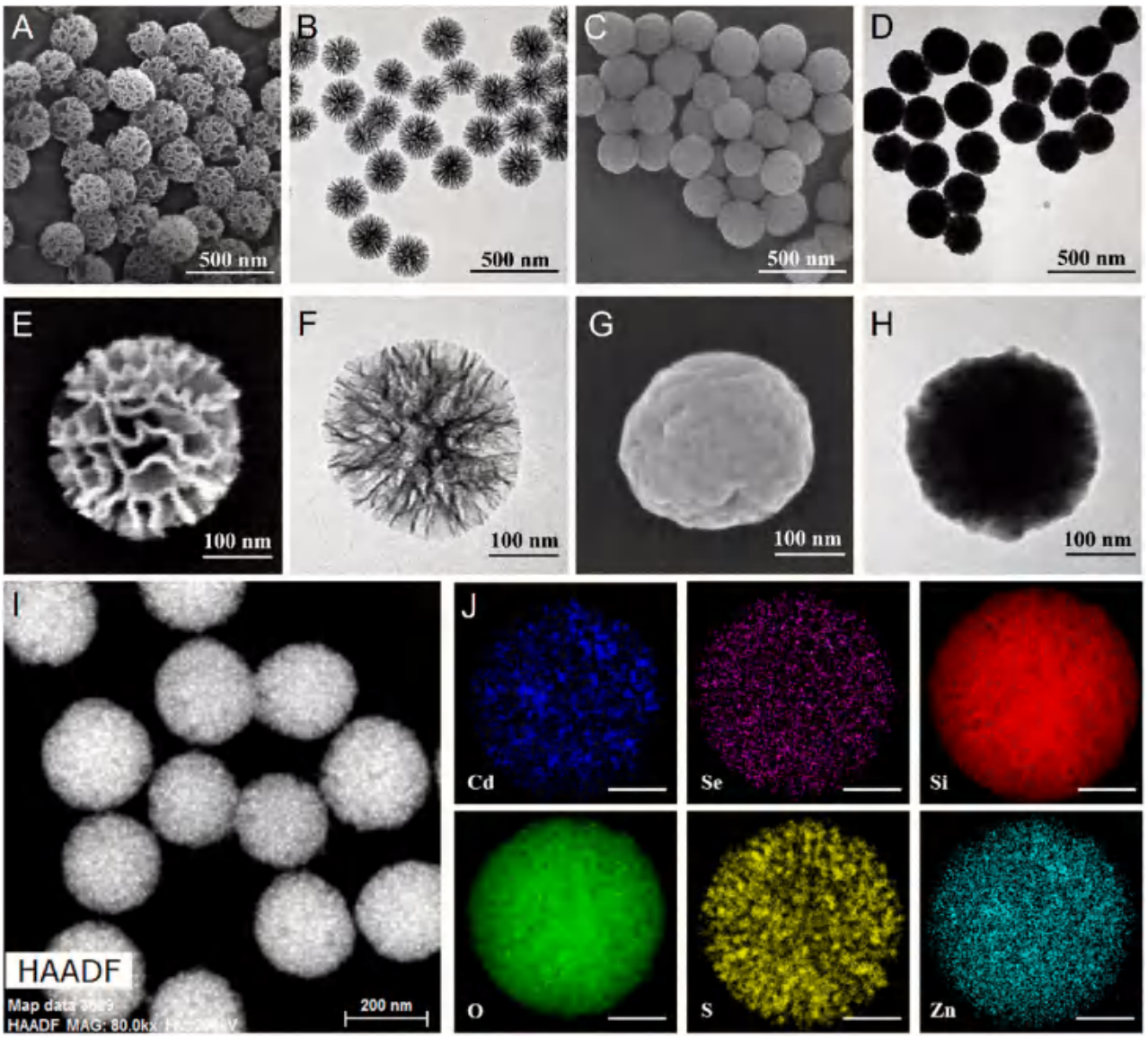

Figure 1. Characterization of DSN and PSS. (A) SEM and (B) TEM images of DSN. (C) SEM and (D) TEM images of PSS. (E, F, G, and H) Magnifications of A, B, C, and D, respectively. (I) STEM-HAADF image and (J) EDS elemental mapping of PSS. Indicated scale bar in J is 80 nm.

25 μL of TEOS and stirred for 2 h. The obtained PSS after centrifugation and washing with ethanol were dispersed in 40 mL of ethanol, added with 1 mL of ammonia and 40 μL of APTES, and reacted for 12 h. The amino-terminated PSS were centrifuged, washed with ethanol, dispersed in 20 mL of DMF containing 5 mg/mL succinic anhydride, and reacted for 4 h. The carboxyl-terminated PSS were washed with ethanol and water several times and dispersed in phosphate buffer saline (PBS, 0.1 M, pH = 6.0) for further use.

Preparation of HAS. The PSS was modified with HRP-Ab2 through the covalent binding between carboxyl and amino groups. Briefly, after incubating PSS with 20 mg/mL EDC and 20 mg/mL NHS for 0.5 h at 25 °C, the solution was supplemented with 10 μL of 7 mg/mL HRP-Ab2 and incubated under stirring for 2.5 h at 25 °C to form the immunosilica spheres (HRP-Ab2-labeled PSS, HAS). HAS was collected by centrifugation and redispersed in PBS (10 mM, pH 7.4 with 0.1% BSA) at 4 °C for further use.

Dual-Modal Immunoassay for RABV Detection. The exact copy number of the virus was determined by quantitative real-time PCR (qRT-PCR).[49] Scheme 1 shows the whole procedure of dual-modal RABV immunoassay. Briefly, 100 μL of 0.25 μg/mL Ab1 was first dropped onto the 96-microwell plate and incubated overnight at 4 °C. After three washes with PBST (1 × PBS buffer containing 0.05% Tween 20, pH 7.4), each well was supplemented with 2% BSA to block the nonspecific active sites, followed by addition of different concentrations of RABV after removing the redundant BSA, and incubation at 37 °C for 1 h. Next, 100 μL of 50 μg/mL HAS was pipetted into the plate through specific binding of antigen and antibody for 1 h at 37 °C. After each well was washed with PBST, 100 μL of pure water was put into each well for fluorescence measurements in the end-point format, while 50 μL of TMB and 50 μL of H_2O_2 were added for colorimetric assays. As the red color of HAS could affect the results of the colorimetric assays, the supernatant was harvested from the immunocomplexes in the 96-microwell plate after catalytic reaction and placed in a new plate for absorbance measurements.

https://dx.doi.org/10.1021/acs.analchem.0c00200
Anal. Chem. XXXX, XXX, XXX−XXX

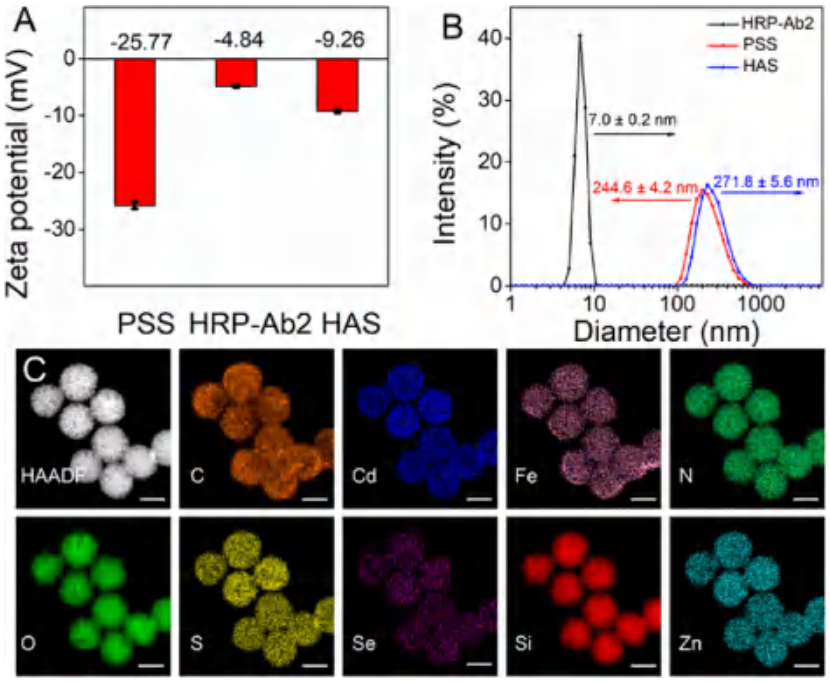

Figure 2. Characterization of HAS. (A) Zeta potentials and (B) dynamic light scattering of PSS, HRP-Ab2, and HAS. (C) EDS elemental mapping of HAS. Indicated scale bar in C is 200 nm.

Dual-Modal RABV Immunoassay in Real Samples. To test the feasibility of the immunoassay in complex matrices, the recovery experiments were performed by spiking different concentrations of RABV into normal cerebrospinal fluid samples obtained from Huazhong Agricultural University (Wuhan, China) and then analyzed by the above method. To further discuss the feasibility of the proposed strategy in clinical applications, the brain tissue samples containing positive and negative samples from mice were collected and tested, including seven RABV-infectious samples and five healthy samples. These samples were tested using the same method as described above. Meanwhile, qRT-PCR detection was also carried out to verify the accuracy and sensitivity of our proposed method.

RESULTS AND DISCUSSION

Characterization of DSN and PSS. Transmission electron microscopy (TEM) and scanning electron microscopy (SEM) were first performed to characterize the synthesized DSN and PSS. As shown in Figure 1A and 1B, the prepared DSN presented a uniform and porous spherical structure with a diameter of 230 nm. In the SEM image (Figure 1E), DSN possessed a pore size of dozens of nanometers. Compared with the carrier of small molecules for bioapplication,[50,51] DSN has the potential of loading nanoparticles or macromolecular drugs. In Figure 1C and 1D, it is shown that the average size of PSS increased to 235 nm, indicating that the thickness of the silica layer was ∼5 nm. The good monodispersity of PSS was probably attributed to the uniform DSN. The large area in the TEM images of DSN and PSS (Figure S1) further illustrated their good monodispersity and uniform morphology. The distribution of each element in the PSS was characterized by high-angle annular dark field (HAADF)-STEM analysis. The STEM-HAADF image revealed the high loading and homogeneous distribution of QDs (Figure 1I), which was used for elemental mapping analysis. Energy-dispersive X-ray spectroscopy (EDS) elemental mapping analysis further showed the presence of Cd, Se, S, and Zn elements within PSS (Figure 1J). In addition, successful synthesis of PSS was further confirmed by elemental composition analysis using X-ray photoelectron spectroscopy (XPS) (Figure S2). Figure S2A presents the wide-scan survey spectrum of PSS, and the characteristic peaks of Zn 2p, C 1s, Cd 3d, O 1s, S 2p, Se 3d, and Si 2p were clearly observed. The energy spectral peaks at 405.05, 53.53, 161.87, and 1021.80 eV, corresponding to Cd 3d, Se 3d, S 2p, and Zn 2p, respectively, were derived from the QDs. These four peaks revealed that QDs were effectively encapsulated in the dendritic silica hosts with an atomic percentage of 1.46% for QDs in PSS as indicated by XPS. The amplified spectra of Zn 2p, C 1s, Cd 3d, O 1s, S 2p, Se 3d, and Si 2p are shown in Figure S2B, S2C, S2D, S2E, S2F, S2G, and S2H, respectively.

The stability of nanoparticles is an important indicator for their application. Herein, the stability of PSS was evaluated by analysis of the two main factors, storage time and pH (Figure S3). The average diameter (Figure S3A) and zeta potential (Figure S3B) remained stable even after 6 weeks of storage, demonstrating the high stability and dispersion of PSS. These results were consistent with the high uniformity and monodispersity indicated by TEM (Figure S1B). Over a storage time of 6 weeks, there was a negligible loss in the fluorescence intensity of PSS (Figure S3C). Moreover, PSS showed excellent fluorescence intensity in the pH range from 3 to 11 (Figure S3D), further revealing its good stability. The high stability of the nanospheres is due to both the passivation of organic ligands and the surface coverage of silica layers, leading to obviously superior stability to that of typical ligand-exchanged QDs.[52]

Characterization of HAS. The zeta potential of these nanospheres was seen to increase dramatically from −25.77 (PSS) to −9.26 mV (HAS) after conjugation with HRP-Ab2 (Figure 2A). The nanospheres were also characterized by

https://dx.doi.org/10.1021/acs.analchem.0c00200
Anal. Chem. XXXX, XXX, XXX−XXX

dynamic light scattering. In Figure 2B, unmodified PSS and HRP-Ab2 are shown to have diameters of 244.6 ± 4.2 and 7.0 ± 0.2 nm, respectively, in contrast to an increase to 271.8 ± 5.6 nm for HAS after modification of HRP-Ab2 on PSS. Furthermore, HRP can be directly evaluated by the presence of the Fe element, and successful synthesis of HAS can be indirectly confirmed by the Fe element in the prepared HAS. EDS elemental mapping revealed the distribution of C, Cd, Fe, N, O, S, Se, Si, and Zn in HAS, demonstrating its successful synthesis (Figure 2C). These results revealed the successful preparation of HAS.

The PL spectra of the PSS after assembly with HRP-Ab2 also maintained identical profiles as those shown in Figure S4A. This PL preservation was verified by time-resolved photoluminescence spectroscopy. The PL decay curve of HAS was almost identical to that of PSS (Figure S4B) with only tiny changes in fitting parameters (Table S1). The strong fluorescence emissions from these nanospheres could be clearly imaged under confocal laser scanning microscopy (CLSM) (Figure S4C and S4D), suggesting their potential applications in analysis and imaging. All of these results indicated that HAS was successfully prepared with a good retention in emission character and high optical stability.

Optimization of Analytical Conditions. To achieve the optimal detection performance of the immunoassay, we examined the effects of various parameters on ELISA performance, including immunoreaction temperature, time, pH value, and BSA concentration. In Figure 3A, the

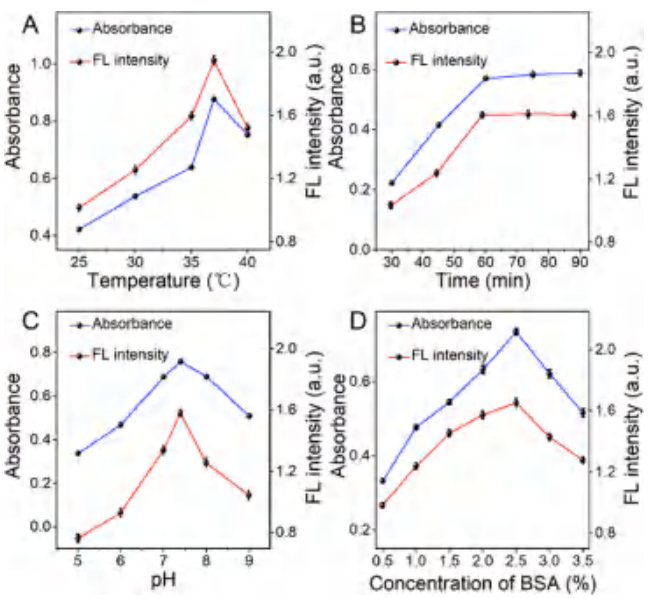

Figure 3. Optimization of parameters in ELISA of temperature (A), immunoreaction time (B), pH value (C), and BSA concentration (D) for colorimetric and fluorescent assays. (Red line) Fluorescence measurements. (Black line) Absorbance measurements.

absorbance and fluorescence intensity values are shown to increase with increasing incubation temperature until reaching 37 °C, followed by a decrease. A possible explanation is that a high or low temperature could not facilitate the binding of antigen and antibody. In Figure 3B, the values were seen to increase with increasing incubation time, followed by a plateau with the incubation time further extending to 90 min. Thus, 60 min was determined as the ideal incubation time to ensure sufficient immunoreaction between antigen and antibody. Figure 3C reveals the two values increased first and then decreased with the increase of pH value. This is probably because a too acidic or too alkaline environment could affect the structure of proteins, destroying their biological activity and influencing the performance of the ELISA. Hence, pH 7.4 was determined as the optimal pH value. Figure 3D shows the effects of different BSA concentrations on the absorbance value and fluorescence intensity. The two values exhibited an increase when the concentration of BSA increased from 0.5 to 2.5%, followed by a decreasing trend above 2.5% BSA, indicating that 2.5% BSA was the proper concentration of blocking agent.

Sensitivity of Dual-Modal Immunoassay. Under optimal conditions, we evaluated the analytical performance of the proposed strategy. The absorption values at 652 nm were intensified with increasing amounts of RABV. A calibration curve was obtained in the detection range from 0.12 to 23.40 ng/mL with a limit of detection of 91 pg/mL (Figure 4A). Meanwhile, the fluorescence signal could be measured even with an ultralow concentration of RABV due to the higher sensitivity of fluorescent assay than the colorimetric assay. A good linear relationship was observed from 0.012 to 46.8 ng/mL with a detection limit of 8 pg/mL (Figure 4B), in contrast to a calculated detection limit of 2.785 ng/mL for conventional ELISA (Figure S5 and Table S2). Thus, the detection limit of our proposed fluorescent and colorimetric method was approximately 348-fold and 30-fold lower than that of the conventional ELISA for RABV detection, respectively (Table S2). Furthermore, the sensitivity of the proposed strategy is equivalent to or even better than that of several reported methods (Table S3). These results indicated the advantages of the proposed dual-modal immunoassay, such as high sensitivity, efficient signal amplification, and wide linear range for convenient prescreening and accurate diagnosis of RABV. Overall, the high sensitivity of the proposed strategy was attributed to the high loading of QDs and HRP-Ab2 for detection probe.

Specificity and Reproducibility of the Immunoassay. The practicability of the proposed dual-modal immunoassay was further tested by evaluating its specificity and reproducibility using RABV, two other canine viruses (canine parvovirus (CPV) and canine distemper virus (CDV)), two proteins such as IgG and BSA, or a mixture of them (Figure 5). Strong signal responses were monitored in the RABV and mixture samples, in contrast to negligible changes in the negative samples, indicating the satisfactory specificity of the designed strategy. The reproducibility was evaluated under the same conditions. The RSD values were 1.75−5.27% for the colorimetric method and 1.36−5.48% for the fluorescent method ($n = 3$), which demonstrated the reliability and practicality of this strategy. In Figure 5, 1−3 represent colorimetric assays and 4−6 represent fluorescence assays. A total of six groups were subject to RABV detection, and the similar strong signal intensities demonstrate the acceptable reproducibility of the immunoassay.

Analysis of RABV Nucleoprotein in Complex Matrices. The reliability and applicability of the proposed strategy was explored by detecting the RABV from the biological media of the mouse cerebrospinal fluid. Specifically, the cerebrospinal fluid of healthy mice was mixed with different concentrations of RABV, and the recoveries of RABV were then recorded with the immunoassay. As shown in Table S4, the recoveries of cerebrospinal fluid samples at different RABV concentrations

https://dx.doi.org/10.1021/acs.analchem.0c00200
Anal. Chem. XXXX, XXX, XXX−XXX

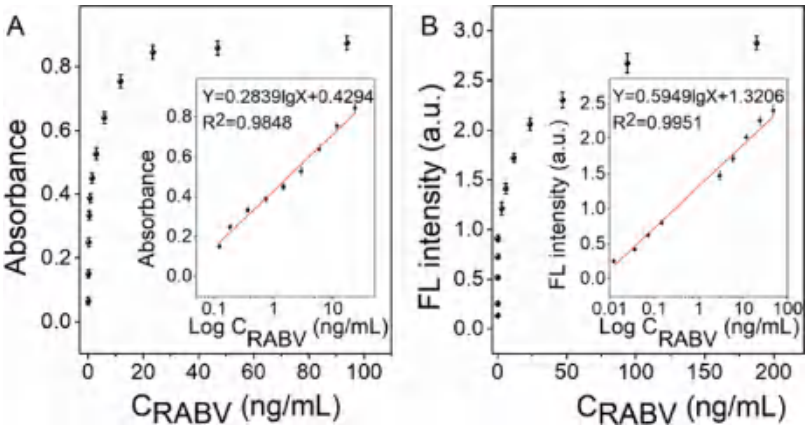

Figure 4. Linear relationship of the dual-modal immunoassay. (A) Absorption values versus different concentrations of RABV with the linear calibration plot in the inset. (B) Fluorescence intensity versus various concentrations of RABV with the linear calibration plot in the inset.

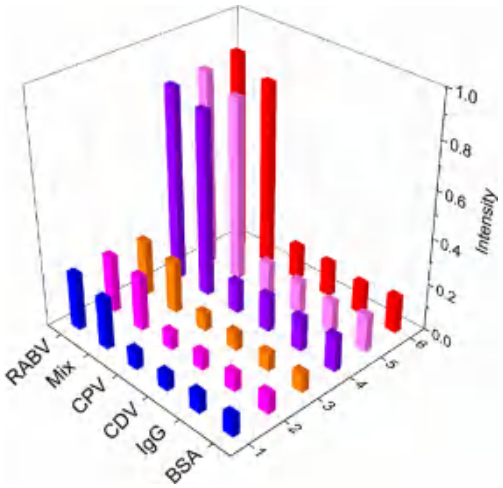

Figure 5. Specificity and reproducibility of the dual-mode measurement. Responses of absorbance value (1−3) and fluorescence intensity (4−6) to BSA, IgG, CDV, CPV, RABV, and the mixture. Concentration was 0.2 ng/mL for RABV and 1 ng/mL for the others.

ranged from 92.22% to 107.78% with RSD values varying from 1.50% to 9.76% for the colorimetric method and from 90.56% to 108.19% with RSD values varying from 2.65% to 8.91% for the fluorescent method, demonstrating the reliability and practicality of this biosensor.

Dual-Modality RABV Immunoassay in Brain Tissue. To further test the reliability and applicability of our dual-modal immunoassay, brain tissue samples were randomly collected from mice for RABV detection. As shown in Figure 6, 6 out of 12 samples were found to be positive via colorimetry because of the absorbance at 652 nm above the threshold value. Encouraged by the higher sensitivity of the fluorescence mode, another sample was diagnosed to be positive, completely consistent with the qRT-PCR results (Figure S6 and Table S5), further verifying the potential applications of our proposed method in real samples. The RSD between colorimetry and fluorescence response was less than 6.8% for the same sample detection, indicating the reliability of the proposed method.

Compared with the traditional single-modal immunoassay, there are several advantages for our HAS-based dual-modal immunoassay. First, our detection system contains both fluorescent and colorimetric signals, which enable the results not only to be prescreened with the naked eye but also to be quantitatively detected by fluorescence signal with enhanced sensitivity. Second, these nanospheres possess superior bright fluorescence, uniform size and shape, and outstanding photostability, endowing them with luminescent properties within the complex environment. Third, this method does not require complicated sample pretreatment or expensive infrastructures, which is user friendly. Finally, our strategy is

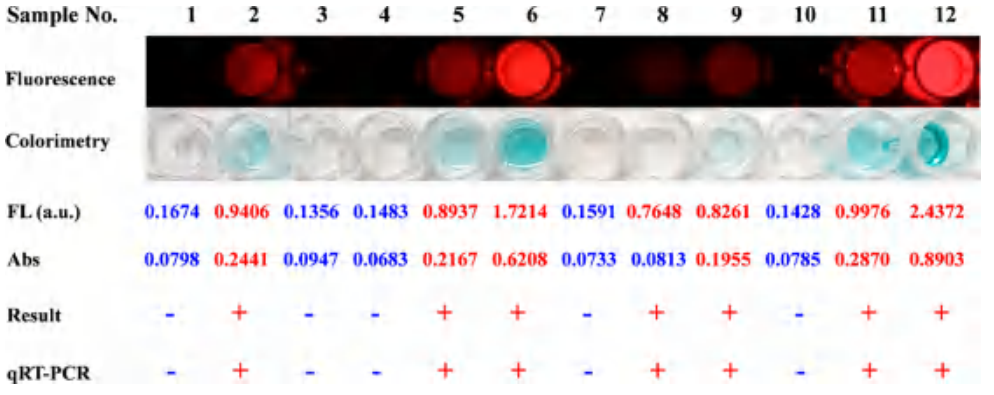

Figure 6. RABV detection of brain tissue samples using our proposed strategy versus qRT-PCR assays. (Blue number) Lower than threshold and is diagnosed to be negative without virus infection risk. (Red number) Higher than threshold and is diagnosed to be positive with virus infection risk. (+) Positive result. (−) Negative result.

https://dx.doi.org/10.1021/acs.analchem.0c00200
Anal. Chem. XXXX, XXX, XXX−XXX

universal and applicable to detection of various targets by changing the antigen and antibody.

CONCLUSIONS

In summary, we presented a simple, sensitive, and selective dual-modal immunoassay for RABV detection based on HAS as the reporter. The dendritic silica nanoparticles incorporate abundant QDs via metal−thiol coordination for production of strong fluorescence signals. In addition, the carboxyl-terminated PSS can provide active groups for antibody conjugation, coupled with colorimetric tags through the specific catalysis of TMB. With the dual-signal readouts of fluorescence and colorimetry, RABV can be preliminarily screened and then accurately diagnosed in complex biological samples. This method can increase the sensitivity by 2−3 orders of magnitude due to the high luminance of PSS with good uniformity. The combined merits of unique DSN, dual-modal readout, high sensitivity, and wide linear range will broaden the applicability of the novel nanoparticles with integrated functions for disease diagnosis.

ASSOCIATED CONTENT

* Supporting Information

The Supporting Information is available free of charge at https://pubs.acs.org/doi/10.1021/acs.analchem.0c00200.

Experimental details; large-area TEM images of DSN and PSS; XPS analysis for PSS; stability of PSS under storage time and pH; PL spectra, PL decay curves, and CLSM images of PSS and HAS; conventional ELISA assay for RABV detection; qRT-PCR analysis for brain tissue samples; biexponential fitting results from fluorescent decay curves of PSS and HAS; comparison of our proposed assay with conventional ELISA for detection of RABV; comparison of the proposed system with other immunosensor for viral detection; standard addition recovery experiments of RABV by the proposed strategy; detection results of 12 brain tissue samples by our dual-modality immunoassay and qRT-PCR (PDF)

AUTHOR INFORMATION

Corresponding Authors

Ling Zhao − State Key Laboratory of Agricultural Microbiology, College of Veterinary Medicine, Huazhong Agricultural University, Wuhan 430070, China; Email: lingzhao@mail.hzau.edu.cn

Heyou Han − State Key Laboratory of Agricultural Microbiology, College of Food Science and Technology, College of Science, Huazhong Agricultural University, Wuhan 430070, China; orcid.org/0000-0001-9406-0722; Email: hyhan@mail.hzau.edu.cn

Authors

Jiaojiao Zhou − State Key Laboratory of Agricultural Microbiology, College of Food Science and Technology, College of Science, Huazhong Agricultural University, Wuhan 430070, China

Meishen Ren − State Key Laboratory of Agricultural Microbiology, College of Veterinary Medicine, Huazhong Agricultural University, Wuhan 430070, China

Wenjing Wang − State Key Laboratory of Agricultural Microbiology, College of Science, Huazhong Agricultural University, Wuhan 430070, China; orcid.org/0000-0003-4035-8552

Liang Huang − College of Chemical Engineering, Zhejiang University of Technology, Hangzhou 310014, China; orcid.org/0000-0002-4789-7068

Zhicheng Lu − State Key Laboratory of Agricultural Microbiology, College of Science, Huazhong Agricultural University, Wuhan 430070, China

Zhiyong Song − State Key Laboratory of Agricultural Microbiology, College of Science, Huazhong Agricultural University, Wuhan 430070, China; orcid.org/0000-0002-2552-5239

Mohamed F. Foda − State Key Laboratory of Agricultural Microbiology, College of Science, Huazhong Agricultural University, Wuhan 430070, China; Department of Biochemistry, Faculty of Agriculture, Benha University, Moshtohor, Toukh 13736, Egypt; orcid.org/0000-0002-2672-1370

Complete contact information is available at: https://pubs.acs.org/10.1021/acs.analchem.0c00200

Author Contributions

§J.Z. and M.R. contributed equally.

Notes

The authors declare no competing financial interest.

ACKNOWLEDGMENTS

We gratefully appreciate the support from the National Natural Science Foundation of China (21778020, 21804046, 21807036, 31750110464, 31950410755) and Sci-tech Innovation Foundation of Huazhong Agriculture University (2662017PY042). We thank Yang Wu and Zhen Wang for help with the TOC figure drawing.

REFERENCES

(1) Hayman, D. T.; Banyard, A. C.; Wakeley, P. R.; Harkess, G.; Marston, D.; Wood, J. L.; Cunningham, A. A.; Fooks, A. R. J. Virol. Methods 2011, 177, 87−93.

(2) Sajjanar, B.; Dhusia, K.; Saxena, S.; Joshi, V.; Bisht, D.; Thakuria, D.; Manjunathareddy, G. B.; Ramteke, P. W.; Kumar, S. Int. J. Biol. Macromol. 2017, 104, 180−188.

(3) Silva, S. R.; Katz, I. S.; Mori, E.; Carnieli, P., Jr.; Vieira, L. F.; Batista, H. B.; Chaves, L. B.; Scheffer, K. C. Biologicals 2013, 41, 217−223.

(4) Hampson, K.; Coudeville, L.; Lembo, T.; Sambo, M.; Kieffer, A.; Attlan, M.; Barrat, J.; Blanton, J. D.; Briggs, D. J.; Cleaveland, S.; Costa, P.; Freuling, C. M.; Hiby, E.; Knopf, L.; Leanes, F.; Meslin, F. X.; Metlin, A.; Miranda, M. E.; Muller, T.; Nel, L. H.; et al. PLoS Neglected Trop. Dis. 2015, 9, e0003709.

(5) Anderson, A.; Shwiff, S. A. Transboundary Emerging Dis. 2015, 62, 446−452.

(6) Organization, W.H. WHO expert consultation on rabies, 3rd report; World Health Organization, 2018.

(7) Faye, M.; Dacheux, L.; Weidmann, M.; Diop, S. A.; Loucoubar, C.; Bourhy, H.; Sall, A. A.; Faye, O. J. Virol. Methods 2017, 243, 120−130.

(8) Mani, R. S.; Madhusudana, S. N. Sci. World J. 2013, 2013, 569712.

(9) Wacharapluesadee, S.; Hemachudha, T. Expert Rev. Mol. Diagn. 2010, 10, 207−218.

(10) Duong, V.; Tarantola, A.; Ong, S.; Mey, C.; Choeung, R.; Ly, S.; Bourhy, H.; Dussart, P.; Buchy, P. Int. J. Infect. Dis. 2016, 46, 107−114.

(11) Wacharapluesadee, S.; Phumesin, P.; Supavonwong, P.; Khawplod, P.; Intarut, N.; Hemachudha, T. J. Virol. Methods 2011, 175, 278−282.
(12) Wacharapluesadee, S.; Tepsumethanon, V.; Supavonwong, P.; Kaewpom, T.; Intarut, N.; Hemachudha, T. J. Virol. Methods 2012, 184, 109−112.
(13) Allendorf, S. D.; Cortez, A.; Heinemann, M. B.; Harary, C. M.; Antunes, J. M.; Peres, M. G.; Vicente, A. F.; Sodre, M. M.; da Rosa, A. R.; Megid, J. Virus Res. 2012, 165, 119−125.
(14) WHO Technical Report Series; WHO, 2005, Vol. 931.
(15) Zhou, J. J.; Wang, W. W.; Li, S. J.; Nie, A. X.; Song, Z. Y.; Foda, M. F.; Lu, Z. C.; Zhao, L.; Han, H. H. Sens. Actuators, B 2020, 304, 127267.
(16) Wang, J. J.; Lin, Y.; Jiang, Y. Z.; Zheng, Z.; Xie, H. Y.; Lv, C.; Chen, Z. L.; Xiong, L. H.; Zhang, Z. L.; Wang, H.; Pang, D. W. Anal. Chem. 2019, 91, 7280−7287.
(17) Zhou, C. H.; Zhao, J. Y.; Pang, D. W.; Zhang, Z. L. Anal. Chem. 2014, 86, 2752−2759.
(18) Qu, W.; Liu, Y.; Liu, D.; Wang, Z.; Jiang, X. Angew. Chem., Int. Ed. 2011, 50, 3442−3445.
(19) Chu, C.; Ge, S.; Zhang, J.; Lin, H.; Liu, G.; Chen, X. Nanoscale 2016, 8, 16168−16171.
(20) de la Rica, R.; Stevens, M. M. Nat. Nanotechnol. 2012, 7, 821−824.
(21) Qing, Z.; Hu, J.; Xu, J.; Zou, Z.; Lei, Y.; Qing, T.; Yang, R. Chem. Sci. 2020, 11, 1985−1990.
(22) Miao, L.; Zhu, C.; Jiao, L.; Li, H.; Du, D.; Lin, Y.; Wei, Q. Anal. Chem. 2018, 90, 1976−1982.
(23) Xie, Q. Y.; Wu, Y. H.; Xiong, Q. R.; Xu, H. Y.; Xiong, Y. H.; Liu, K.; Jin, Y.; Lai, W. H. Biosens. Bioelectron. 2014, 54, 262−265.
(24) Mei, J.; Leung, N. L.; Kwok, R. T.; Lam, J. W.; Tang, B. Z. Chem. Rev. 2015, 115, 11718−11940.
(25) Luo, J.; Xie, Z.; Lam, J. W. Y.; Cheng, L.; Tang, B. Z.; Chen, H.; Qiu, C.; Kwok, H. S.; Zhan, X.; Liu, Y.; Zhu, D. Chem. Commun. 2001, 18, 1740−1741.
(26) Jun, S.; Lee, J.; Jang, E. ACS Nano 2013, 7, 1472−1477.
(27) He, Y.; Lu, H. T.; Sai, L. M.; Su, Y. Y.; Hu, M.; Fan, C. H.; Huang, W.; Wang, L. H. Adv. Mater. 2008, 20, 3416−3421.
(28) Selvan, S. T.; Tan, T. T.; Ying, J. Y. Adv. Mater. 2005, 17, 1620−1625.
(29) Liu, Q.; Guo, B.; Rao, Z.; Zhang, B.; Gong, J. R. Nano Lett. 2013, 13, 2436−2441.
(30) Zrazhevskiy, P.; Sena, M.; Gao, X. Chem. Soc. Rev. 2010, 39, 4326−4354.
(31) Dai, X.; Zhang, Z.; Jin, Y.; Niu, Y.; Cao, H.; Liang, X.; Chen, L.; Wang, J.; Peng, X. Nature 2014, 515, 96−99.
(32) Yang, Z. C.; Wang, M.; Yong, A. M.; Wong, S. Y.; Zhang, X. H.; Tan, H.; Chang, A. Y.; Li, X.; Wang, J. Chem. Commun. 2011, 47, 11615−11617.
(33) Zhou, J.; Yang, Y.; Zhang, C. Y. Chem. Commun. 2013, 49, 8605−8607.
(34) Li, Z.; Wang, G.; Shen, Y.; Guo, N.; Ma, N. Adv. Funct. Mater. 2018, 28, 1707152.
(35) Hong, S.-L.; Zhang, Y.-N.; Liu, Y.-H.; Tang, M.; Pang, D.-W.; Wong, G.; Chen, J.; Qiu, X.; Gao, G. F.; Liu, W.; et al. Anal. Chem. 2018, 90, 7310−7317.
(36) Kokkinos, C.; Angelopoulou, M.; Economou, A.; Prodromidis, M.; Florou, A.; Haasnoot, W.; Petrou, P.; Kakabakos, S. Anal. Chem. 2016, 88, 6897−6904.
(37) Qiu, Z.; Shu, J.; Tang, D. Anal. Chem. 2017, 89, 5152−5160.
(38) Ashiba, H.; Sugiyama, Y.; Wang, X.; Shirato, H.; Higo-Moriguchi, K.; Taniguchi, K.; Ohki, Y.; Fujimaki, M. Biosens. Bioelectron. 2017, 93, 260−266.
(39) Takemura, K.; Adegoke, O.; Takahashi, N.; Kato, T.; Li, T.-C.; Kitamoto, N.; Tanaka, T.; Suzuki, T.; Park, E. Y. Biosens. Bioelectron. 2017, 89, 998−1005.
(40) Li, Q.; Yin, W.; Li, W.; Zhang, Z.; Zhang, X.; Zhang, X. E.; Cui, Z. Nano Lett. 2018, 18, 7457−7468.
(41) Ma, Y.; Wang, M.; Li, W.; Zhang, Z.; Zhang, X.; Tan, T.; Zhang, X. E.; Cui, Z. Nat. Commun. 2017, 8, 15318.
(42) Qin, C.; Li, W.; Li, Q.; Yin, W.; Zhang, X.; Zhang, Z.; Zhang, X. E.; Cui, Z. Proc. Natl. Acad. Sci. U. S. A. 2019, 116, 2577−2582.
(43) Chen, G.; Zhu, J. Y.; Zhang, Z. L.; Zhang, W.; Ren, J. G.; Wu, M.; Hong, Z. Y.; Lv, C.; Pang, D. W.; Zhao, Y. F. Angew. Chem., Int. Ed. 2015, 54, 1036−1040.
(44) Sun, X.; Li, W.; Zhang, X.; Qi, M.; Zhang, Z.; Zhang, X. E.; Cui, Z. Nano Lett. 2016, 16, 6164−6171.
(45) Kim, M. W.; Jeong, H. Y.; Kang, S. J.; Choi, M. J.; You, Y. M.; Im, C. S.; Lee, T. S.; Song, I. H.; Lee, C. G.; Rhee, K. J.; Lee, Y. K.; Park, Y. S. Sci. Rep. 2017, 7, 9474.
(46) Qian, J.; Zhang, C.; Cao, X.; Liu, S. Anal. Chem. 2010, 82, 6422−6429.
(47) Chen, L.; Chen, C.; Li, R.; Li, Y.; Liu, S. Chem. Commun. 2009, 19, 2670−2672.
(48) Yang, Y.; Bernardi, S.; Song, H.; Zhang, J.; Yu, M.; Reid, J. C.; Strounina, E.; Searles, D. J.; Yu, C. Chem. Mater. 2016, 28, 704−707.
(49) Tian, B.; Zhou, M.; Yang, Y.; Yu, L.; Luo, Z.; Tian, D.; Wang, K.; Cui, M.; Chen, H.; Fu, Z. F.; Zhao, L. Front. Immunol. 2018, 8, 2011.
(50) Liu, G. D.; Wang, J.; Wu, H.; Lin, Y. H. Anal. Chem. 2006, 78, 7417−7423.
(51) Pan, L.; He, Q.; Liu, J.; Chen, Y.; Ma, M.; Zhang, L.; Shi, J. J. Am. Chem. Soc. 2012, 134, 5722−5725.
(52) Yoon, M.; Kim, Y.; Cho, J. ACS Nano 2011, 5, 5417−5426.

https://dx.doi.org/10.1021/acs.analchem.0c00200
Anal. Chem. XXXX, XXX, XXX−XXX